Nanosecond Photolysis of Rhodopsin: Evidence for a New, Blue-Shifted Intermediate†

Stephan J. Hug, James W. Lewis, Cora M. Einterz, Thorgeir E. Thorgeirsson, and David S. Kliger*
Chemistry Department, University of California, Santa Cruz, California 95064
Received June 6, 1989; Revised Manuscript Received October 3, 1989

ABSTRACT: Early photolysis intermediates of native bovine rhodopsin (RHO) are investigated by nanosecond laser photolysis near physiological temperature. Absorption difference spectra are collected after excitation with 477-, 532-, and 560-nm laser pulses of various energies and with 477-nm laser excitation at 5, 12, 17, 21, and 32 °C. The data are analyzed by using singular-value decomposition (SVD) and a global exponential fitting routine. Two rate constants associated with distinct spectral changes are observed during the time normally associated with the decay of bathorhodopsin to lumirhodopsin. Various models consistent with this observation are considered. A sequential model in which there is a reversible step between a bathorhodopsin intermediate and a new intermediate (BSI), which is blue-shifted relative to lumirhodopsin, is shown to best fit the data. The temperature dependence of the observed and calculated rate constants leads to linear Arrhenius plots. Extrapolation of the temperature dependence suggests that BSI should not be observable after rhodopsin photolysis at temperatures below −100 °C. The results are discussed with regard to the artificial visual pigments *cis*-5,6-dihydroisorhodopsin and 13-demethylrhodopsin. It is proposed that the rate of the BATHO to BSI transition is limited by the relaxation of the strained *all-trans*-retinal chromophore within a tight protein environment. The transition to LUMI involves chromophore relaxation concurrent with protein relaxation. While the first process is strongly affected by changes in the chromophore, the second transition seems to be determined more by protein relaxation.

Absorption of light by rhodopsin (RHO)[1] leads to an isomerization of the 11-*cis*-retinylidene chromophore to an all-trans conformation in less than 12 ps (Doukas et al., 1981, 1985). The primary photoproduct, prebathorhodopsin (Peters & Leontis, 1982; Peters et al., 1977) or photorhodopsin (Shichida et al., 1984), decays on a time scale of 10^{-11} s to bathorhodopsin (BATHO) [for recent reviews of the primary process and later intermediates see Ottolenghi and Sheves (1987) and Shichida (1986)]. BATHO is the first intermediate that is stable at low temperature (below 133 K), and it has a lifetime in the range of 10^{-8}–10^{-7} s at room temperature. Much of the attention devoted to BATHO is due to its property of storing ~32 kcal/mol photon energy (Boucher & Leblanc, 1985; Cooper, 1979; Schick et al., 1987). This energy is used in subsequent transitions which ultimately lead to an activated form of the protein which catalyzes the visual transduction process. There has also been considerable interest in the cause for the red shift of the BATHO absorption maximum relative to that of RHO (530–540 nm in BATHO compared to 500 nm in RHO). The exact mechanism of energy storage and the origin of the bathochromic shift are presently unclear. The emerging picture is that BATHO stores energy via conformational strain in the chromophore and electrostatic interactions between the chromophore and the protein. The next well-characterized intermediate, lumirhodopsin (LUMI), has a room temperature lifetime on the order of 10^{-5} s and is stable up to 200 K. FTIR data (Rothschild & DeGrip, 1986) indicate that the chromophore strain in LUMI has relaxed and that protein changes, which are already present at the BATHO stage, have significantly increased.

Detailed investigation of the BATHO to LUMI transition at low temperature and at room temperature has shown that this process is more complicated than the decay of a single BATHO species to a single LUMI. Multiple forms of BATHO and LUMI were first observed at low temperature (Yoshizawa & Wald, 1963; Grellman et al., 1962). At room temperature, the BATHO to LUMI transition in RHO and in isorhodopsin (ISO) involves two rate constants with distinct spectral changes (Einterz et al., 1987a; Hug et al., 1987). Since low-temperature studies suggested that two forms of BATHO were formed in parallel at low temperature (Sasaki et al., 1980), the room temperature kinetic data were analyzed in terms of a parallel decay of two BATHO products to the same or to two distinct LUMI products. With this analysis, the slower decaying component ($BATHO_1$) had a lifetime of 170 ± 20 ns and a minimum in the $LUMI_1$ – $BATHO_1$ difference spectrum at 565 nm. The faster decaying component ($BATHO_2$) had a lifetime of 36 ± 15 ns and a $LUMI_2$ – $BATHO_2$ minimum at 535 nm.

In order to understand the nature of the BATHO products, nanosecond photolysis experiments have been performed on various artificial pigments made by introducing synthetically modified retinals into opsin. The first intermediate (BSI) observed in the room temperature, nanosecond photolysis study of the pigment *cis*-5,6-dihydroisorhodopsin (5,6-diH-ISORHO) was blue-shifted relative to the second intermediate, identified as the LUMI intermediate (Albeck et al., 1989). No red-shifted intermediate comparable to what would be expected for a BATHO intermediate was observed on a nanosecond time scale. In comparing lifetimes, absorption

† We thank the National Institutes of Health for support of this work through Grant EY00983.

[1] Abbreviations: BATHO, bathorhodopsin; BSI, blue-shifted intermediate; FP, final product, i.e., the thermally stable photoproduct of rhodopsin in the presence of 1% Ammonyx LO; ISORHO, isorhodopsin; RHO, rhodopsin; LUMI, lumirhodopsin; 5,6-diH-ISORHO, pigment formed from opsin and *cis*-5,6-dihydro-9-*cis*-retinal; 4,5-deH-5,6-diH-ISORHO, pigment formed from opsin and 4,5-deH-*cis*-5,6-dihydro-9-*cis*-retinal; 13-dm-RHO, pigment formed from opsin and 13-demethyl-11-*cis*-retinal; SVD, singular value decomposition.

0006-2960/90/0429-1475$02.50/0

maxima, and low-temperature stabilities of the 5,6-diH-ISORHO intermediates with those of RHO, it was suggested that the blue-shifted intermediate (or BSI) was a decay product of BATHO. It was argued that BATHO of 5,6-diH-ISORHO decays too fast to be seen on a nanosecond time scale due to fast chromophore relaxation resulting from decreased rigidity in the cyclohexene ring. Similar observations were made with other artificial pigments including 4,5-deH-5,6-diH-ISORHO. Interesting results were also found with a pigment formed from bovine opsin and 11-*cis*-13-demethylretinal (13-dm-RHO). Here absorption maxima are observed both to the blue of LUMI (similar to the BSI intermediate described above) and to the red of the parent pigment (similar to a BATHO species) at early times following photolysis [following paper (Einterz et al., 1990)].

No clear evidence of a blue-shifted intermediate has been seen in spectra of RHO at low temperatures or in room temperature spectra when a mechanism involving the parallel decay of the two early intermediates was used to analyze nanosecond photolysis data (although the $BATHO_2 - LUMI_2$ difference spectrum arising from a parallel decay appears to yield a blue-shifted LUMI). However, since blue-shifted intermediates have been observed in several artificial pigments, it is natural to question whether a blue-shifted intermediate between the BATHO and LUMI intermediates could also be formed upon photolysis of RHO. This led us to question whether a model assuming parallel decay of early photolysis intermediates is justified and, if not, whether other models would reveal a BSI-like intermediate upon photolysis of RHO.

To answer these questions, we pursued two approaches. First, we measured the spectra of the early photolysis intermediates upon excitation of RHO at different wavelengths with varying laser powers in order to test the parallel model. At high laser powers, significant amounts of the intermediates present at early times are photolyzed to produce ISO by the 7-ns fwhm laser pulse. Since the $BATHO_1$ and $BATHO_2$ species are spectrally distinct, we should observe varying ratios of the two intermediates as a function of laser power and wavelength if both species are present during the laser pulse (i.e., if they are both formed rapidly and decay in parallel). While preliminary results (Einterz et al., 1987b) at a single wavelength encouraged a parallel model, the lack of a wavelength-dependent $BATHO_1/BATHO_2$ ratio in more extensive measurements described below suggests that the two species are not both present at early times.

Since the assumption of a parallel decay of early photolysis intermediates was in question, alternative models were tested. To do this, we conducted time-resolved spectral measurements at various temperatures and analyzed the data with a global fitting procedure to determine which models best explain all spectra simultaneously. Various models were considered and are discussed below.

Experimental Procedures

Samples consisted of suspensions of 1 mg/mL rhodopsin from hypotonically washed rod outer segments (ROS) solubilized in 2% octyl glucoside solution (Lewis et al., 1984). Photolysis experiments were performed as described previously except that the sample cell was modified so its temperature could be controlled. This was accomplished by using a copper insert in the cell which could be cooled or heated by flowing liquid from a thermostated bath. The path length through the sample was 10 mm for the probe beam (cross section 1 mm × 2 mm) and 2 mm for the exciting beam (cross section 1 mm × 10 mm). The laser beam entered the sample at an angle of 90° from the probe beam, and the laser polarization was set at magic angle (54.7°) with respect to the probe polarization in order to eliminate time-dependent spectral artifacts due to rotational relaxation effects. The sample was replaced after each laser pulse by a flow system using a syringe whose plunger was controlled by a computer-driven stepper motor. Samples were photolyzed by 7-ns (fwhm), 0.7–0.8-mJ pulses of 477-nm light from a Quanta Ray DCR-2 Nd:YAG pumped dye laser. Different wavelengths and laser energies were used for the wavelength and power dependence measurements as indicated below. Optical difference spectra were measured with a gated (10-ns) optical multichannel analyzer system as described previously (Einterz et al., 1987a; Lewis et al., 1987). In order to determine absolute spectra of the photolysis intermediates, a bleaching difference spectrum, from which the amount of RHO bleached and the amount of ISO formed by each laser pulse could be calculated, was obtained as described previously (Albeck et al., 1989).

Global Analysis

The optical difference spectra collected at successive times between 20 and 1000 ns exhibit isosbestic points which shift with time as shown previously (Einterz et al., 1987a). This behavior cannot be explained by a process in which a single species exponentially decays to another distinct species. At least two different processes with different rates must be present. In our previous work, we complemented the optical difference data by measuring absorption kinetics at fixed wavelengths with a resolution of 2 ns. Only at two wavelengths, the isosbestic points for the slow and the fast processes, could the kinetic curves by accurately fit by single exponentials. The lifetimes measured at these wavelengths were then used to calculate intermediate spectra by assuming parallel decay of the intermediates. Here we will analyze this data using a global fit approach, where the data at all wavelengths and all times are simultaneously fit to a multiexponential process. This approach makes kinetic measurements at one wavelength unnecessary and is more general in the sense that the minimal number of exponentially decaying intermediates needed to fit all the spectra can be determined in an unbiased way. The global analysis indicates, as we concluded earlier, that only two decay processes are needed to explain the spectral data. When a parallel decay mechanism is assumed, both methods give the same results, within experimental error, for data presented in earlier work.

Global Exponential Fitting. A global exponential fitting of the optical difference spectra (ΔOD spectra) collected at different times following excitation was performed by using an adaption of methods described by Nagle and Lozier and by Hofrichter (Nagle et al., 1982; Hofrichter et al., 1985). Generally, a number of ΔOD spectra of a system evolving with first-order rate constants can be described by

$$\Delta OD(\lambda,t) = \sum_{i=1}^{k} b_i(\lambda) \exp(-tk_i) \quad (1)$$

where the k_i's are the observed rate constants and the b_i spectra are the corresponding spectral changes. For the analysis of RHO data, a time-independent term b_0, associated with $k_0 = 0$, is introduced. The b_0 spectrum contains the spectra of all photoproducts that appear stable during the time over which the ΔOD spectra were collected (including any ISO formed upon photolysis minus the fraction of RHO that is bleached). Thus

$$\Delta OD(\lambda,t) = \sum_{i=0}^{k} b_i(\lambda) \exp(-tk_i) \quad (2)$$

By collecting ΔOD spectra at n times, with each spectrum

consisting of optical density values at m wavelengths, $\Delta OD(\lambda,t)$ represents an $m \times n$ matrix. The right side of expression 2 is given by a product of two matrices **BT**. **B** is an $m \times (k + 1)$ matrix, where the $k + 1$ columns consist of the $b_i(\lambda)$ spectra. **T** is a $(k + 1) \times n$ matrix, where each row describes the exponential decay of each corresponding $b_i(\lambda)$ spectrum. An exponential fitting program must thus find the **B** and **T** matrices that best fit the ΔOD values in a least-squares sense, so that the total sum of the squared residuals $[(\Delta OD - \mathbf{BT})^2]$ over all times and all wavelengths is minimized. **B** contains $m(k + 1)$ linear parameters, and **T** contains k exponential parameters. In the data described here, m is 180, so that if k is 2, a fitting program must find 540 linear parameters and 2 exponential parameters.

The singular-value decomposition approach (SVD) provides a very efficient way to speed up the fitting procedure and to determine the number of spectrally distinct intermediates. It can also be used to eliminate random noise from the data. According to the SVD theorem, the $m \times n$ ΔOD matrix can be written as the product of three matrices: $\Delta OD = \mathbf{USV}^T$ (Golub, 1970). Considering only the columns associated with nonzero eigenvalues, **U** is an $m \times n$ matrix whose columns are the so-called basis spectra. **S** is an $n \times n$ diagonal matrix containing positive decreasing eigenvalues. **V** is an $n \times n$ matrix describing the composition of the original matrix in terms of the basis spectra. The importance of the basis spectra in terms of fitting the data in a least-squares sense varies as the square of their eigenvalues. Typically, only the first few (o, where $o < n$) basis spectra are needed to represent a data matrix; all the other basis spectra contain random noise. In more mathematical terms, o is the lowest rank approximation to the data matrix to within the signal to noise of the experiment. It gives the minimal number of linearly independent (orthogonal) basis spectra (columns of **U**) that are needed to represent the data matrix. The representation of a large data matrix thus becomes the product of three much smaller matrices, and the whole time correlation of the data is contained in the $n \times o$ **V** matrix. Equation 2 can then be written as

$$\Delta OD(\lambda,t) = \mathbf{USV}^T = \mathbf{BT} \quad (3)$$

Since the ΔOD spectra can be written as a linear combination of columns of **B** as well as by a linear combination of columns of the product **US**, the columns of **B** can also be written as a linear combination of columns of **US**. Taking a matrix **C** which performs this linear combination, eq 3 becomes

$$\Delta OD(\lambda,t) = \mathbf{USV}^T = \mathbf{USCT} \quad (4)$$

Multiplying by $\mathbf{U}^{-1}$ and by $\mathbf{S}^{-1}$, the exponential fitting problem is reduced to

$$\mathbf{V}^T = \mathbf{CT} \quad (5)$$

Realizing that $\mathbf{V}^T$ is an $o \times n$ matrix, that **C** is an $o \times (k + 1)$ matrix, that **T** is a $(k + 1) \times n$ matrix, and that o is usually much smaller than n (3 in the ΔOD data presented here), the drastic simplification of the exponential fit becomes obvious. Instead of $(k + 1)m$ parameters, there are now only $(k + 1)o$ linear parameters to be fit. For the data presented here, this means 9 linear parameters instead of 540! Once the **C** matrix and the rate constants are found, the $b_i(\lambda)$ spectra can be calculated by

$$\mathbf{B} = \mathbf{USC} \quad (6)$$

The fitting procedure used pseudoinverses for a least-squares fit of the linear parameters in **C** and a simplex routine for the least-squares fit of the exponential rate constants. The fits were performed on an IBM-PC using Matlab[2] software. Two-exponential fits required 30–60 s on a 80386-based machine. Up to five exponential fits were performed on test data, taking about 10 min to converge.

Model-Dependent Calculations of Intermediate Spectra. The b spectra obtained from SVD analyses are related to spectra of intermediates in a model-dependent way. The simplest relation is found in the case of a parallel decay of k intermediates to k other intermediates. Here, each k_i is the rate constant for the decay of intermediate i into its new intermediate, and the b spectra are the difference spectra between the decaying and the appearing intermediates. For example, if we have two BATHO products decaying to two LUMI products according to

$$\mathrm{BATHO}_2 \xrightarrow{k_1} \mathrm{LUMI}_2$$

$$\mathrm{BATHO}_1 \xrightarrow{k_2} \mathrm{LUMI}_1$$

where k_1 and k_2 are equal to the observed rate constants, then the observed ΔOD as a function of time is given by

$$\Delta OD = \mathrm{BATHO}_2 \exp(-tk_1) + \mathrm{LUMI}_2[1 - \exp(-tk_1)] + \mathrm{BATHO}_1 \exp(-tk_2) + \mathrm{LUMI}_1[1 - \exp(-tk_2)] + (-\mathrm{RHO} + \mathrm{ISO})$$

where –RHO, BATHO, and ISO stand for the decrease of RHO absorption and increase of absorptions of BATHO and ISO produced at zero time by the laser pulse and LUMI stands for the absorption of LUMI after the total conversion of BATHO into LUMI. The assignments of the subscripts 1 and 2 are made so that they are consistent with previous experiments. This can be rewritten as

$$\Delta OD = (-\mathrm{RHO} + \mathrm{ISO}) + \mathrm{LUMI}_1 + \mathrm{LUMI}_2 + [\exp(-tk_1)](\mathrm{BATHO}_2 - \mathrm{LUMI}_2) + [\exp(-tk_2)](\mathrm{BATHO}_1 - \mathrm{LUMI}_1)$$

By comparison of this expression with eq 2 it can be seen that

$$b_0 = (-\mathrm{RHO} + \mathrm{ISO}) + \mathrm{LUMI}_1 + \mathrm{LUMI}_2$$

$$b_1 = \mathrm{BATHO}_2 - \mathrm{LUMI}_2$$

$$b_2 = \mathrm{BATHO}_1 - \mathrm{LUMI}_1$$

For other models, the spectra of the intermediates are linear combinations of the b spectra, so that for each model there is a matrix **K** that converts the b spectra into the intermediate spectra.

Results

Wavelength and Power Dependence. Parallel Model. During the excitation of RHO with a 7-ns fwhm laser pulse, BATHO is formed within picoseconds and upon further absorption of light can form RHO or ISO according to

$$\mathrm{RHO} \underset{0.25}{\overset{0.67}{\rightleftharpoons}} \mathrm{BATHO} \underset{0.20}{\overset{0.05}{\rightleftharpoons}} \mathrm{ISO}$$

The quantum yields above and below the arrows (Kliger et al., 1984; Hurley et al., 1977; Suzuki & Callender, 1981) refer to the overall photolysis of BATHO, whether BATHO consists of one or several forms. The laser pulses used in our experiments lead to ISO formation which was dependent on the laser wavelength and the laser energy.

The amount of ISO formed relative to the amount of RHO that is absent after the laser pulse (the RHO that is absent has formed either BATHO or ISO) can be calculated from the bleaching difference spectrum (Albeck et al., 1989). This

[2] The Math Works, Inc., 20 North Main St., Suite 250, Sherborn, MA 01770.

is the difference spectrum between the octyl glucoside solubilized RHO sample before and seconds after laser excitation under conditions identical with those used to measure intermediate spectra, except that a small amount (1%) of Ammonyx LO (Onyx Chemical, New Jersey) was added to the RHO sample to ensure complete bleaching. Under these conditions the bleached RHO which became BATHO has decayed to a stable final product (FP) with Ammonyx.

The bleaching difference spectrum consists of absorption contributions from −RHO + ISO + FP. The −RHO + ISO part (denoted as BLEACH) is the spectrum that has to be added to the ΔOD spectra to obtain the OD spectra. The % ISO formed relative to the RHO absent after the laser pulse is then calculated as 100(ISO/RHO). Depending on laser power and wavelength, between 10% and 45% ISO was formed. Since the quantum yield for photolysis of BATHO to RHO is 5 times larger than for photolysis to ISO, most of the initially formed BATHO is back-photolyzed to RHO.

Excitation of RHO with laser pulses of different wavelengths and energies should reveal whether one or several spectrally distinct BATHO products are present during the laser pulse. If a parallel model is appropriate to explain the biexponential decay of BATHO in our experiments, two spectrally distinct BATHO's, $BATHO_1$ and $BATHO_2$, would be formed during the laser pulses. From the $BATHO_1$ − $LUMI_1$ and $BATHO_2$ − $LUMI_2$ spectra it can be seen that $BATHO_1$ has a red-shifted absorption relative to $BATHO_2$. In changing the laser excitation from 477 to 532 nm and finally to 560 nm, relatively more $BATHO_1$ should be photolyzed and the ratio of $BATHO_1/BATHO_2$ should decrease. This effect should furthermore increase in going from low laser power to higher laser power. Figure 1 shows the BATHO − LUMI spectra obtained after excitation at the different wavelengths with low laser pulse energies (ca. 0.5 mJ/pulse, Figure 1A) and with high laser pulse energies (ca. 2 mJ/pulse, Figure 1B). The spectra have been scaled to constant $BATHO_1$ − $LUMI_1$ amplitudes for easier comparison. The amounts of ISO formed at low and at high powers are 15% and 23% at 477 nm, 35% and 45% at 532 nm, and 10% and 32% at 560 nm. Within the signal to noise, there is no wavelength or power dependence of the $BATHO_1/BATHO_2$ ratio. While it is difficult to predict exactly how much the $BATHO_1/BATHO_2$ ratio should change without detailed knowledge of the spectra, quantum yields, and transition dipole moment directions of the two hypothetical BATHO's, it is clear from examining a few likely values that only an extraordinary coincidence could result in invariant relative amplitudes over the range of wavelengths and powers used here.

These observations lead to serious questions about a parallel model. No effect of laser wavelength or laser power would be observed in sequential models, where only one BATHO is present during the laser pulse. We thus investigated the possibility that a sequential model of BATHO decay is a viable alternative.

Sequential Models. (A) Calculation of Intermediate Spectra and Criteria for Acceptable Models. As mentioned above, the *b* spectra obtained from global exponential fits of ΔOD data are directly related to intermediate difference spectra of parallel decaying intermediates. For other models there are matrices **K** that convert the *b* spectra into intermediate difference spectra (intermediate − BLEACH spectra).

To test the validity of any particular model, experimental conditions can be changed in ways that lead to predictable changes which can confirm or discredit a proposed model. Since the power and wavelength dependence studies did not support a parallel model, we conducted a temperature dependence study and considered alternative (sequential) models. Several criteria were used to test for the validity of a particular model.

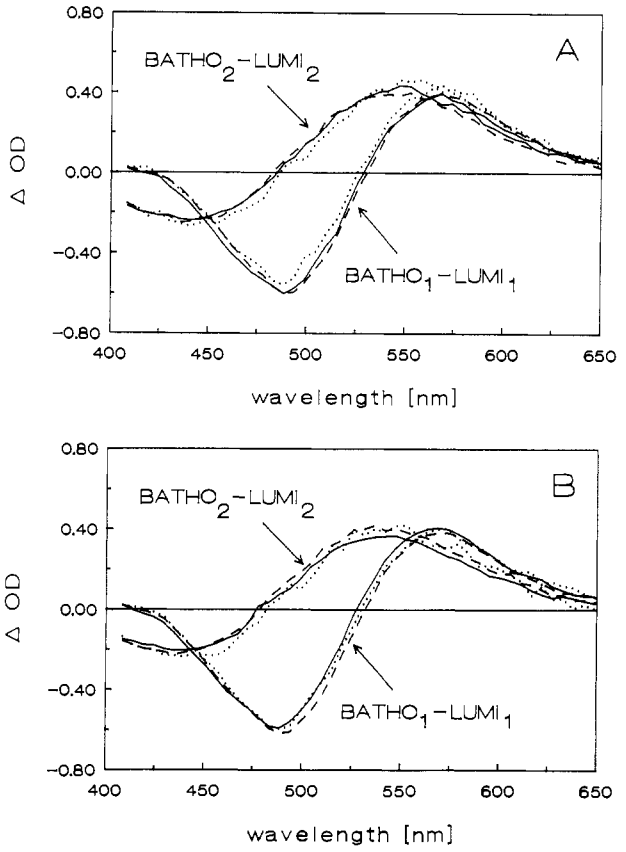

FIGURE 1: Test of a parallel model by power and wavelength dependence. The relative amplitudes of the $BATHO_1$ − $LUMI_1$ and the $BATHO_2$ − $LUMI_2$ spectra as a function of the wavelength and power of the exciting laser pulse are compared. The spectra are scaled to constant peak to peak amplitudes of the $BATHO_1$ − $LUMI_1$ spectra. (—) 477 nm; (- - -) 532 nm; (···) 560 nm. Panel A shows excitation with laser pulse energies of 0.4–0.5 mJ/pulse, and panel B, with 1.8–2.2 mJ/pulse. The relative amplitudes remain the same within signal to noise and thus do not support a parallel model where $BATHO_1$ and $BATHO_2$ are present during the laser pulse.

These criteria were that the calculated intermediate spectra are well-behaved in the sense that they reveal no negative absorptions, that the spectra should be temperature independent in shape and amplitude (spectra reported here are taken over the range of 5–32 °C), and that the spectra should yield smooth absorption curves with only one maximum and should exhibit a log-normal shape, a shape that has been observed for all rhodopsin intermediates at room temperature and at low temperature. Finally, an additional criterium is that the Arrhenius plots of the rate constants produced from the analyses are linear over the temperature interval studied.

For a sequential model, where BATHO decays into a new intermediate X, which then decays into LUMI, according to

$$\text{BATHO} \xrightarrow{k_1} \text{X} \xrightarrow{k_2} \text{LUMI} \qquad \text{(SEQ1)}$$

the concentrations of the intermediates as a function of time are given by

$$[\text{BATHO}] = c_0 \exp(-tk_1)$$

$$[\text{X}] = c_0\{[k_1/(k_2 - k_1)] \exp(-tk_1) - [k_1/(k_2 - k_1)] \exp(-tk_2)\} \quad (7)$$

$$[\text{LUMI}] = c_0\{1 - [k_2/(k_2 - k_1)] \exp(-tk_1) + [k_1/(k_2 - k_1)] \exp(-tk_2)\}$$

where c_0 is the initial concentration of BATHO formed by the laser pulse. Note that for generality we refer to the second intermediate in the sequential models as X at this point but will show under Discussion that it is similar to the BSI intermediate previously found in artificial pigments. If ϵ_B, ϵ_X, and ϵ_L are defined as the molar extinction coefficient spectra of the intermediates, $\Delta OD(t,\lambda)$ is given by

$$\Delta OD/c_0 = (\epsilon_L - \epsilon_{BLEACH}) + [\exp(-tk_1)]\{\epsilon_B + [k_1/(k_2 - k_1)]\epsilon_X + [-k_2/(k_2 - k_1)]\epsilon_L\} + [\exp(-tk_2)]\{[-k_1/(k_2 - k_1)]\epsilon_X + [k_1/(k_2 - k_1)]\epsilon_L\} \quad (8)$$

By comparison of eq 8 with eq 2, the expressions in the braces give the b spectra in terms of the intermediate spectra and the rate constants. This can be written as a matrix equation, where the matrix **K** in the center converts the intermediate spectra into the b spectra:

$$\begin{bmatrix} b_0 \\ b_1 \\ b_2 \end{bmatrix} = \begin{bmatrix} 0 & 0 & 1 \\ 1 & k_1/(k_2 - k_1) & -k_2/(k_2 - k_1) \\ 0 & -k_1/(k_2 - k_1) & k_1/(k_2 - k_1) \end{bmatrix} \begin{bmatrix} c_0(\epsilon_B - \epsilon_{BLEACH}) \\ c_0(\epsilon_X - \epsilon_{BLEACH}) \\ c_0(\epsilon_L - \epsilon_{BLEACH}) \end{bmatrix}$$

The intermediate − BLEACH spectra can thus be obtained by multiplying the b spectra with $\mathbf{K}^{-1}$. In this expression the b spectra and the intermediate − BLEACH spectra are written as row vectors.

Two more complex models, in which reversible steps between the first (BATHO) and the second (X) intermediates are introduced, were also considered. These are

$$\text{BATHO} \underset{k_{21}}{\overset{k_{12}}{\rightleftharpoons}} \text{X} \xrightarrow{k_{23}} \text{LUMI} \qquad \text{(SEQ2)}$$

and

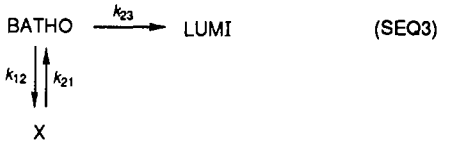

The **K** matrices for these models were derived from integrated rate laws taken from Bamford and Tipper (1969). The real rate constants k_1 and k_2 in model SEQ1 are equal to the observed rate constants k_1 and k_2 obtained from the global exponential fit. For the models SEQ2 and SEQ3, the real rate constants, k_{12}, k_{21}, and k_{23} are calculated from the observed rate constants k_1 and k_2 and from the equilibrium constants K_{eq} defined as k_{12}/k_{21}. The equilibrium constants can be determined from the temperature dependence and the requirement that the resulting intermediate spectra be temperature independent, as will be described below.

(B) Temperature Dependence of Spectra. The measured ΔOD spectra at 5, 21, and 32 °C and at seven times between 20 and 1000 ns following photolysis are shown in Figure 2. SVD and global exponential analysis of these data indicated that they could all be fit by two-exponential processes. This was shown by the fact that the residuals (actual data minus biexponential fit) showed no wavelength-dependent structure but only consisted of random noise. Three-exponential fits led either to nonconvergence of the fitting routine or to unreasonable lifetimes and b spectra, with no improvement of the residuals. This indicates that LUMI is a stable photoproduct and that two other intermediates preceed the formation of LUMI over the time domain of our analysis. The observed lifetimes for the fast and the slow processes leading to LUMI formation are given in the first two columns of Table I.

Figure 3 shows the b spectra for data collected at 5, 21, and 32 °C. The spectra have been scaled to a constant amplitude of the b_0 spectra for easier comparison. (This was necessary because the laser pulse energy varied slightly in experiments carried out at the different temperatures.) It is obvious that the b_1 spectrum shows a marked temperature dependence. Its amplitude increases by about 30% in going from 5 to 32 °C. Since the b spectra are directly related to a parallel model as described above, this would mean that the partition ratio of the decay from a common precursor into two BATHO products would have to be temperature dependent or that there is a temperature-dependent equilibrium prior to the BATHO intermediates. Below we present the intermediate spectra obtained by applying the different decay mechanisms consistent with two observed rate constants and discuss their viability according to the criteria discussed above.

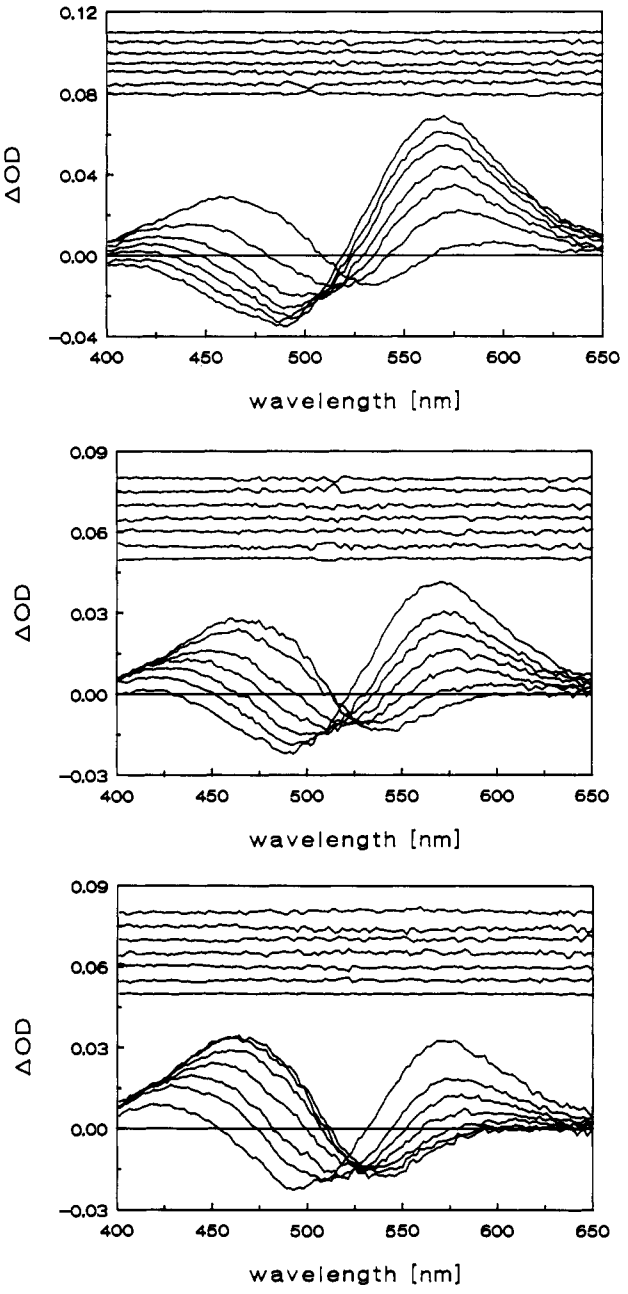

FIGURE 2: Transient difference spectra of detergent-solubilized RHO after photolysis with 7-ns fwhm 477-nm laser pulses at 5 °C (top), 21 °C (middle), and 32 °C (bottom). The spectra were collected at 20, 40, 70, 120, 250, 600, and 1000 ns after photolysis (corresponding to curves of decreasing absorption in the red and increasing absorption in the blue). The shifting isosbestic points indicate kinetics that are more complicated than single exponential. Shown above the spectra are the corresponding residuals (actual data minus two-exponential fit). They are offset from zero for each curve for clarity. (Increasing times are shown from bottom to top.)

Table I: Inverses of Observed and Real Rate Constants at Different Temperatures[a]

temp (°C)	$1/k_{1,obs}$	$1/k_{2,obs}$	$1/k_{12}$	$1/k_{21}$	$1/k_{23}$	K_{eq} (k_{12}/k_{21}) method 1	K_{eq} (k_{12}/k_{21}) method 2
5	92	719	225	225	292	1	1.04
12	54	327	118	155	150	1.32	1.31
17	41	267	85	117	129	1.38	1.40
21	36	215	74	107	105	1.45	1.44
32	16	92	29	51	49	1.73	1.69

[a] Observed and calculated inverse rate constants (ns) and the equilibrium constants (see text) for the model

$$\text{BATHO} \underset{k_{21}}{\overset{k_{12}}{\rightleftharpoons}} \text{BSI} \xrightarrow{k_{23}} \text{LUMI}$$

The estimated error bounds of the observed lifetimes are ±10% or not less than 7 ns. The estimated error bounds for the calculated inverse rate constants are ±20%.

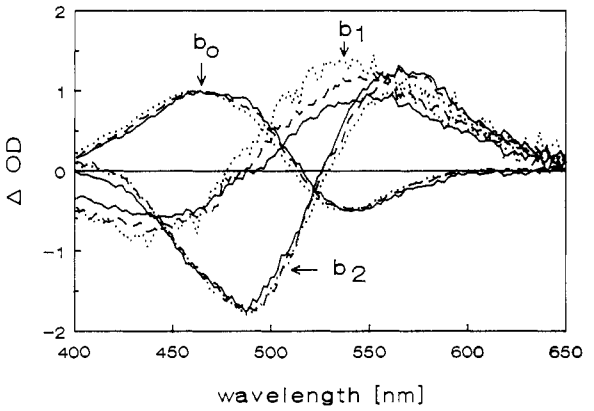

FIGURE 3: *b* spectra (preexponential factors) resulting from analysis of the transient difference spectra at 5 °C (—), 21 °C (---), and 32 °C (···). The spectra are scaled to constant amplitudes of b_0. They are used to calculate the intermediate spectra for sequential models as explained in the text. In a parallel model, the b_1 spectra correspond to the $BATHO_2$ – $LUMI_2$ spectra and the b_2 spectra to the $BATHO_1$ – $LUMI_1$ spectra.

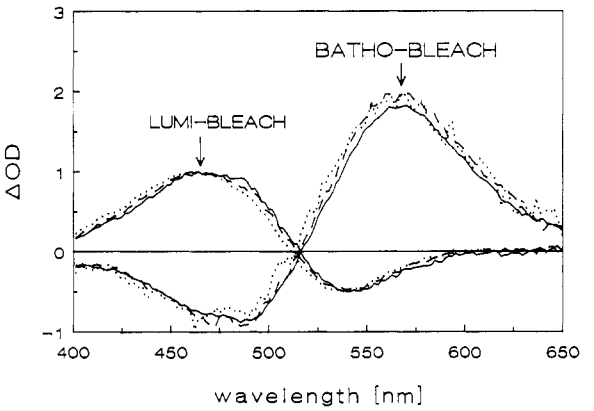

FIGURE 4: Intermediate difference (intermediate – BLEACH) spectra of BATHO and LUMI at 5, 21, and 32 °C, obtained from the scaled *b* spectra of Figure 3 after applying sequential models. The models SEQ1, SEQ2, and SEQ3 (see text) give the same spectra for the BATHO and LUMI intermediates. (—) 5 °C; (---) 21 °C; (···) 32 °C.

Figure 4 shows two of the intermediate – BLEACH spectra, BATHO – BLEACH and LUMI – BLEACH, calculated for the simple sequential model SEQ1. These spectra fulfill the criteria for an acceptable model; they are basically temperature independent within signal to noise. On the other hand, the spectrum of the second intermediate, shown in Figure 5A, shows a marked temperature dependence. The absorption in the blue increases with increasing temperature while the absorption in the red decreases.

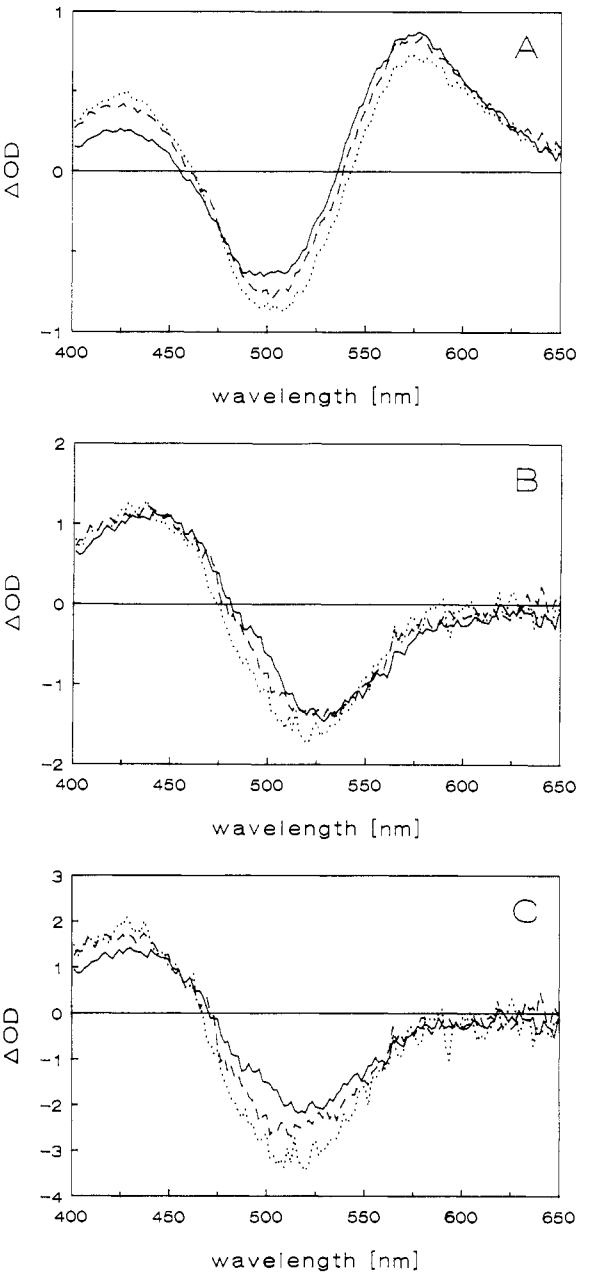

FIGURE 5: Intermediate difference spectra of X (BSI) at 5, 21, and 32 °C. Panel A shows spectra obtained with SEQ1, panel B shows spectra obtained with SEQ2, and panel C shows spectra obtained with SEQ3. The spectra in panel B show the least systematic temperature dependence. The model SEQ2 (BATHO ⇄ BSI → LUMI) thus satisfies the requirement of producing temperature-independent intermediates best. (—) 5 °C; (---) 21 °C; (···) 32 °C.

This calls model SEQ1 into question and led us to consider models SEQ2 and SEQ3 in which we introduce reversible steps between the BATHO and X intermediates. This means that the spectra presented in Figure 5A are actually the spectra of different mixtures of the first and the second intermediates. Applying models SEQ2 and SEQ3 has the effect that the first intermediate spectrum (BATHO) is subtracted from that of the second intermediate spectrum (X) which would be found assuming no reverse rate constant. The spectra of the first and the last intermediate (BATHO and LUMI, Figure 4) are not affected by using models SEQ2 and SEQ3 instead of SEQ1.

To find the equilibrium constants that lead to an X intermediate spectrum which is least temperature dependent, we

used two different methods. In the first method (method 1), we started with data at the lowest temperature and chose an equilibrium constant that led to subtraction of as much of the first intermediate as possible without causing negative absorptions in the intermediate spectra obtained after the addition of the BLEACH spectrum. The remaining equilibrium constants were found by a simplex program so that the least-squares deviation of the spectra at all five temperatures from the average spectrum was minimized. Figure 5B,C shows the difference spectra of the second intermediate for models SEQ2 and SEQ3, with equilibrium constants at the lowest temperature set to 1.0 for SEQ2 and to 0.3 for SEQ3. Lower values lead to negative absorptions; higher values basically mean incomplete subtraction of the first intermediate. The spectrum of the second intermediate is noisy, but considering the signal-to-noise ratio, the spectrum in Figure 5B (model SEQ2) contains the least systematic changes with temperature.

In the second, more rigorous method (method 2), we used an SVD approach similar to the one used for the global exponential fit of the ΔOD spectra to determine the equilibrium constants. SVD was performed on the entire set of *b* spectra collected at five different temperatures. The eigenvalues obtained in this way indicated that only three basis spectra were needed to reproduce all the 5 × 3 *b* spectra to within our signal to noise. (This supports the use of three intermediates.) These three significant basis spectra were then used to find the three temperature-independent intermediate spectra that best fit the 3 × 5 *b* spectra after multiplication with the **K** matrices for the three sequential models. The residuals (differences between the *b* spectra from the global exponential fits and the *b* spectra reconstructed from the temperature-independent intermediate spectra) can then be compared for different models. This allows an unbiased comparison (without prior assumptions of any equilibrium constants) of how well a certain model fits the data. The coefficients for the construction of the intermediate spectra from the basis spectra were found by use of pseudoinverses, and the equilibrium constants for the models SEQ2 and SEQ3 were simultaneously optimized by a simplex routine. The intermediate spectra found with method 2 for the models SEQ1 and SEQ2 are almost identical with the average of the spectra obtained with method 1, and the equilibrium constants for model SEQ2 converged to basically the same values (Table I, last two columns).

For the model SEQ3, the equilibrium constants converged to very small values which, after addition of the BLEACH, lead to intermediate spectra with large negative values. No equilibrium constants could be found that lead to more temperature-independent intermediate spectra than those shown in Figure 5C without causing negative absorptions. Model SEQ3 can thus be discounted.

The residuals (*b* spectra obtained from the global exponential fit minus the *b* spectra calculated from the optimized intermediate difference spectra) resulting from model SEQ2 were more random than those resulting from model SEQ1. The intermediate difference spectra and the intermediate spectra (with added BLEACH) optimized by method 2 for model SEQ2 are shown in panels a and b, respectively, of Figure 6. The absorption maxima for the three intermediates as obtained from log-normal fits are as follows: BATHO, 529 nm; X, 477 nm; and LUMI, 492 nm.

The observed and the calculated real rate constants as well as the equilibrium constants at five temperatures are summarized in Table I. All of the rate constants show good Arrhenius behavior as can be seen in Figures 7 and 8. Both models SEQ1 and SEQ2 fulfill the requirement of producing

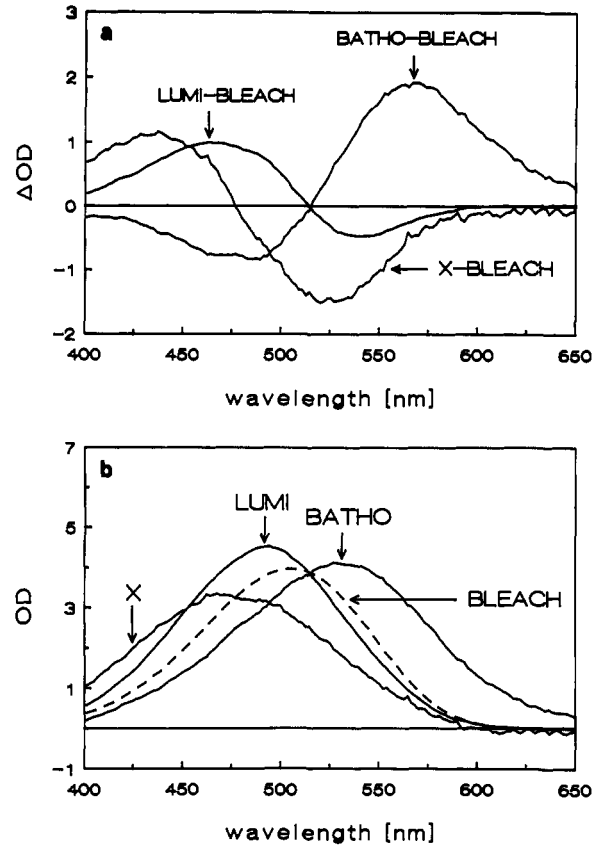

FIGURE 6: (a) Temperature-independent intermediate difference spectra of model SEQ2 that best fit the *b* spectra obtained at different temperatures (see text). They are basically equal to the averages of the spectra shown in Figures 4 and 5B. (b) Corresponding intermediate spectra where the BLEACH spectrum (also shown) has been added. The absorption maxima for the intermediates as obtained from log-normal fits are as follows: BATHO, 529 nm; X, or BSI, 477 nm; and LUMI, 492 nm.

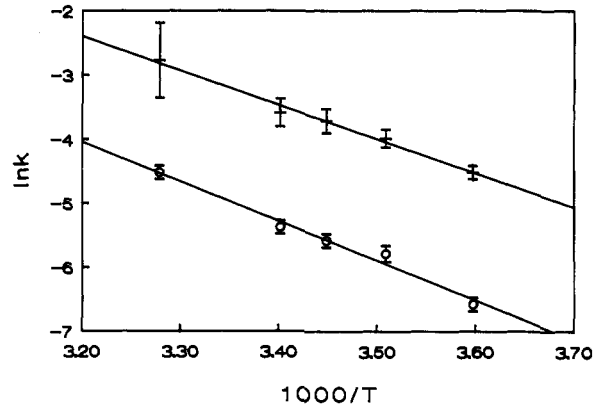

FIGURE 7: Arrhenius behavior of the observed rate constants [(+) k_1; (O) k_2] with estimated errors. The activation energies are 10.6 kcal/mol for k_1 and 12.3 kcal/mol for k_2. The units of the rate constants are ns^{-1}.

nonnegative and well-behaved intermediate spectra and also lead to linear Arrhenius plots. Model SEQ2 performs better than SEQ1 in producing temperature-independent intermediate spectra.

Further support for a sequential decay mechanism that includes a reversible step between BATHO and X comes from measurements of the polarization of the intermediate spectra (Lewis et al., 1989). Analysis of these polarization experiments yielded a polarization ratio that varied across the absorption band of the second intermediate when a sequential model without a reversible step was used but yielded constant po-

Table II: Inverses of Observed and Real Rate Constants (in min) Extrapolated to Low Temperatures[a]

temp (K)	$1/k_{1,obs}$	$1/k_{2,obs}$	$1/k_{12}$	$1/k_{21}$	$1/k_{23}$	$(k_{12}/k_{21})(1000)$
120	145	59200	19700	9.94	438	0.504
130	4.76	1120	373	0.53	14.3	1.41
140	0.253	37.4	12.5	0.043	0.762	3.45
150	0.019	1.96	0.653	0.0049	0.06	7.45

[a] Inverse observed and inverse calculated rate constants (assuming model SEQ2) at low temperatures obtained from extrapolation of the Arrhenius plots. Discrepancies between the observed and the real rate constants are due to the extrapolation over the large temperature region. The equilibrium constants (k_{12}/k_{21}) indicate that BSI cannot be observed at low temperature.

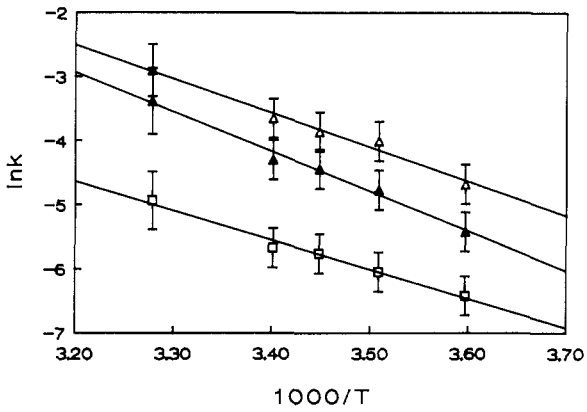

FIGURE 8: Arrhenius behavior of the calculated rate constants for the model SEQ2. Activation energies and symbols are as follows: (▲) k_{12} = 12.3 kcal/mol; (□) k_{21} = 9.1 kcal/mol; (△) k_{23} = 10.6 kcal/mol. The units of the rate constants are ns^{-1}. The values for k_{21} and k_{23} are offset by −1 and +1 units on the ln k axis, respectively, for clarity.

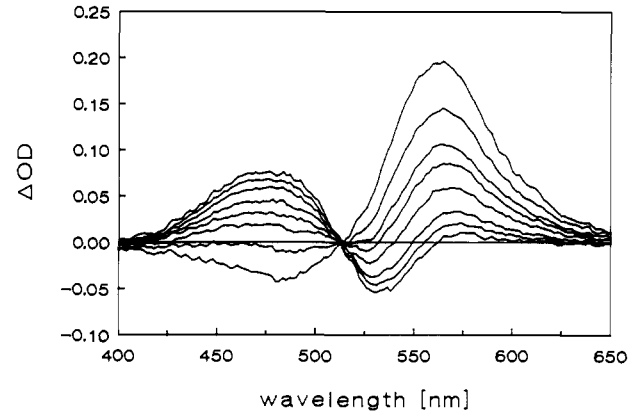

FIGURE 9: Optical difference spectra of detergent-solubilized RHO in glycerol/water (2:1) at 160 K. The spectra were measured at 0, 0.82, 1.4, 1.9, 2.9, 5.1, 8.5, and 14.9 min after irradiation with light between 430 and 480 nm for 60 s (with successive spectra showing decreased absorptions in the red and increased absorptions in the blue). In contrast to measurements at room temperature, a sharp isosbestic point is observed. The observed optical changes agree well with the prediction that a decay from BATHO into LUMI with only a negligible formation of BSI should be observed.

larizations across the intermediate bands with the inclusion of a reversible step.

(*C*) *Extrapolation to Low Temperatures.* Another test for the proposed sequential model with a reversible step is the extrapolation of the Arrhenius plots to low temperatures and the comparison of the predicted behavior with actual measurements. Table II shows the extrapolation of the rate constants to low temperatures. Here, k_1 and k_2 are the extrapolated observed rate constants, and k_{12}, k_{21}, and k_{23} are the extrapolated real rate constants for the model SEQ2. At low temperature, the sum of $k_{12} + k_{21}$ is much larger than k_{23} so that the observed rate constants have the meaning that k_1 is the rate at which a steady-state equilibrium between BATHO and BSI is established, while k_2 is the rate at which the equilibrium decays to LUMI. Often cited in low-temperature spectroscopy of RHO intermediates are transition temperatures at which, upon warming of the sample, a transition from one intermediate into the next intermediate occurs. For the following arguments, we define the transition temperatures as the temperatures at which a transition occurs with an inverse rate (lifetime) of less than 30 min. (Lifetimes below 30 min make the measurement of a spectrum with a conventional scanning spectrometer difficult.) From Table II, the inverse rate constants predict two transitions, the first occurring between 120 and 130 K (not observable as described below), the second between 140 and 150 K.

We conducted experiments where detergent-solubilized RHO in a water/glycerol (1:3) mixture was irradiated at 160 ± 5 K with light between 420 and 480 nm for 30–60 s. The spectral changes were then followed by collecting spectra over 15 min following irradiation. The time to collect one spectrum was 15 s. The resulting ΔOD spectra displayed a sharp isosbestic point (Figure 9). The observed lifetime was on the order of minutes, in good agreement with the extrapolation. Reliable exponential fits were not possible here, because the temperature was not stabilized sufficiently well to warrant reliable rate constants over the time the spectra were collected. At 155–165 K only the second transition can be observed, since the first transition at this temperature is fast and is completed during irradiation. Model SEQ2 predicts that the first transition is not observable even at lower temperature, because the equilibrium constant k_{12}/k_{21} is so small that only an undetectable amount of BSI is formed. All that could be observed is the second transition, which is the decay from BATHO + BSI in a steady-state equilibrium to LUMI. But since the fraction of BSI is undetectably small, this appears like a transition from BATHO to LUMI. From the intermediate spectra in Figure 6b, an isosbestic point at about 515 nm with an OD close to zero is predicted. This is very close to what is observed experimentally (Figure 9). Also, the transition temperature for the BATHO to LUMI decay near 140 K is in good agreement with the 133 K cited by Yoshizawa et al. (1963).

Discussion

Both the wavelength and power dependence as well as the temperature dependence data indicate that a sequential model explains the observed biexponential ΔOD data. Of three sequential models considered, a model with a reversible step between BATHO and X, which then decays into LUMI, comes closest to fulfilling the requirement of temperature-independent intermediate spectra. More complicated models, such as one that would also include a reversible step between X and LUMI, were not considered because the spectrum of LUMI was temperature independent. This would not be the case if there was a temperature-dependent reversible rate constant of the same order of magnitude between LUMI and X. Furthermore, the existing data do not warrant consideration of more complicated models involving additional ad-

justable parameters. The reasons that the proposed model does not perfectly fit the observed data (some remaining temperature dependence of the intermediate – bleach spectra, Figure 5B) could be experimental (pulse duration of 7 ns, magic angle deviations, timing) or could be due to the possibility that the intermediate spectra are not absolutely temperature independent. The model is strongly supported by the excellent Arrhenius behavior, by agreement with predictions for low-temperature spectra, and by observations in polarization studies (Lewis et al., 1989). It should, however, be pointed out that refinements of the proposed model could become necessary when detailed experiments over larger temperature regions are conducted. For example, two forms of BATHO could be in a steady-state equilibrium at 160 K and above but could become two distinguishable intermediates at lower temperature.

Interestingly, the spectrum of the X intermediate is very similar in terms of its blue shift from the parent pigment to the BSI intermediates observed in several artificial visual pigments (Albeck et al., 1989; Einterz et al., 1990). It appears that various structural changes in the chromophore affect the kinetics of the BATHO decay but that BSI is a common intermediate in all of them. We will thus refer to this X intermediate in the remainder of this paper as BSI.

Interesting energetic conclusions can be drawn from the activation energies and from the temperature dependence of the equilibrium constants. The activation energy (E_a) for the first transition, BATHO → BSI, is approximately 12.3 kcal/mol, E_a of the reverse transition BSI → BATHO is around 9.1 kcal/mol, and E_a for the BSI → LUMI transition is approximately 10.6 kcal/mol. This indicates that the BSI intermediate lies higher in energy than BATHO by about 3 kcal/mol. It also indicates that the first transition becomes the rate-limiting step at low temperature and that the steady-state equilibrium concentration of BSI becomes very small, as is reflected in the low-temperature extrapolations.

One might question why a BSI intermediate has not been observed before. In room temperature experiments this is reasonable because spectral measurements with high enough signal-to-noise ratio to observe such an intermediate have only recently become available. The BSI intermediate would be difficult to observe at low temperatures because of the small steady-state equilibrium concentration of BSI at low temperature.

The observation of a blue-shifted intermediate poses interesting questions about the mechanism of BATHO relaxation. It is now well accepted that BATHO contains an isomerized all-trans chromophore (Akita et al., 1980; Mao et al., 1981; Fukada et al., 1984; Hubbard & Kropf, 1958; Rosenfeld et al., 1977; Eyring et al., 1980, 1982; Sheves et al., 1986). However, the resonance Raman spectrum of BATHO shows unusually intense hydrogen out-of-plane (HOOP) wagging vibrations in the 800–920-cm^{-1} region, attributed to the $C_{10}H$, $C_{11}H$, $C_{12}H$, and $C_{14}H$ wags, which indicates that the chromophore is conformationally distorted (Eyring et al., 1980, 1982). Strong perturbations in the C_8–C_9 and C_{14}–C_{15} stretching frequencies also suggest a distortion in the central region of the chromophore which may account for a substantial part of the energy storage in BATHO (Palings et al., 1987; Birge & Hubbard, 1980; Warshel & Barboy, 1982). It has also been suggested that a negative counterion is not associated with the imine proton but lies underneath the plane of the chromophore interacting with the C_{13} and C_{15} positions of the chromophore. In this model, 40% of the energy storage in BATHO would arise from charge separation (Birge et al., 1988).

In addition to these chromophore distortions, FTIR studies have detected small peptide backbone changes as early as the BATHO stage. These changes have significantly increased at the LUMI stage, while the HOOP vibrations between 800 and 920 cm^{-1} have disappeared and a new HOOP mode is present that is closer to the normal frequency of an all-trans protonated retinylidene molecule (DeGrip et al., 1987; Rothschild & DeGrip, 1986). The transition from BATHO to LUMI thus involves a relaxation of the chromophore to a more relaxed all-trans conformation via conformational changes in both the retinal and in the protein.

Photolysis experiments with artificial pigments have been very valuable in assessing the influence of structural changes in the chromophore on the photointermediates. In 5,6-diH-ISORHO, BSI is formed in less than 7 ns at room temperature and no red-shifted intermediate was observed. It was suggested that saturation of the 5,6-double bond affects the retinal–protein interactions at the BATHO stage by changing the ring–chain and/or the ring–5-methyl conformation (Albeck et al., 1989). Consequently, the initially formed 5,6-diH-BATHO is destabilized and undergoes a fast change in the retinal conformation which results in the BSI intermediate. The BSI intermediate then decays with a lifetime of 100–200 ns (similar to the BSI in RHO) into its corresponding LUMI intermediate.

A similar destabilization of the BATHO intermediate could also explain the observations made with the pigment 13-dm-RHO. Room temperature photolysis of 13-dm-RHO produces an intermediate with a very broad spectrum with a maximum to the blue of the parent pigment and a lower intensity extension to the red within less than 7 ns. This intermediate decays with a lifetime of 100 ns (again close to BSI in RHO) to an intermediate with an absorption maximum closer to the parent pigment, which we identify as LUMI (Einterz et al., 1990).

These results show that the absence of a 5,6-double bond or the absence of a 13-methyl group leads to a much faster formation of the BSI intermediates than is the case in RHO. While in the 5,6-diH-ISORHO the formation of BSI from BATHO is fast and complete, there are indications that in 13-dm-RHO there is a reversible step between BATHO and BSI as in RHO but that a steady-state equilibrium in 13-dm-RHO is established within less than 7 ns at room temperature. While the rate of formation of BSI is strongly affected by changes in the chromophore, the decay rates of the BSI are very similar in RHO, 5,6-diH-ISORHO, and 13-dm-RHO. We suggest that this process is largely limited by conformational changes in the protein, which allow a release of chromophore strain. The formation of BSI must involve significant changes in the chromophore conformation or in the electrostatic environment, given the large spectral shift from BATHO to BSI. These changes are apparently more hindered in native RHO than in the artificial pigments where either a 5,6-double bond or the 13-methyl group has been removed. The temperature dependence of the rate constants between BATHO and BSI shows that the energy of BSI in native RHO lies about 3 kcal/mol above the energy of BATHO. Corresponding energies for the 5,6-diH-ISORHO and the 13-dm-RHO pigments have not been determined. The observation that the equilibrium in these pigments favors the BSI intermediates at room temperature and at low temperature suggests that the energy of BSI in these pigments is lower. The formation of BSI in native RHO might thus be associated with increased steric and/or electrostatic interactions between the chromophore and the protein, forced by movements of the

13-methyl group and ring–chain interaction.

It would obviously be interesting to relate the large spectral shifts associated with the BATHO to LUMI transition [BATHO(529) → BSI(477) → LUMI(492)] to structural changes in the chromophore. However, no definite suggestion can be made at this time, since at present even the spectra of RHO and ISO, and especially the basic red shift in BATHO, are not fully understood. Several factors, such as external protein charges (Derguini & Nakanishi, 1986; Honig et al., 1979a,b; Birge et al., 1988), Schiff base–counterion and H-bond interactions (Sheves et al., 1987, 1985; Lugtenburg et al., 1986; Spudich et al., 1986), and single-bond rotations (Shichida et al., 1981), may participate in determining the spectrum of the above blue-shifted intermediates. It is known that double-bond twisting generally leads to red shifts, while single-bond twisting leads to blue shifts (Becker, 1988). In this context it is possible that at the BATHO stage steric interactions with the protein induce twists of double bonds in the chromophore while at the BSI stage distortions are moved more to single-bond twists. On the other hand, electrostatic interactions could also lead to the observed spectral shifts. The possible presence of a counterion underneath the chromophore plane could induce charge redistributions when conformational changes in the chromophore occur. FTIR and resonance Raman studies would be instrumental in assessing the structure of BSI. The observation of the BSI intermediate of RHO is, however, complicated by the fact that BSI cannot be stabilized at low temperature. Transient resonance Raman measurements at room temperature should be able to reveal new vibrations appearing after formation of BATHO and disappearing concurrent with the formation of LUMI.

ACKNOWLEDGMENTS

We thank J. Hofrichter, R. H. Lozier, M. Ottolenghi, and J. F. Nagle for helpful discussions.

Registry No. *all-trans*-Retinal, 116-31-4.

REFERENCES

Akita, H., Tanis, S. P., Adams, M., Balogh-Nair, V., & Nakanishi, K. (1980) *J. Am. Chem. Soc. 102*, 6370–6372.

Albeck, A., Friedman, N., Ottolenghi, M., Sheves, M., Einterz, C. M., Hug, S. J., Lewis, J. W., & Kliger, D. S. (1989) *Biophys. J. 55*, 233–241.

Bamford, C. H., & Tipper, C. F. H. (1969) *Comprehensive Chemical Kinetics*, pp 29–32, Elsevier Publishing Co., Amsterdam, London, and New York.

Becker, R. (1988) *Photochem. Photobiol. 48* (3), 369–399.

Birge, R. R., & Hubbard, L. M. (1980) *J. Am. Chem. Soc. 102*, 2195–2205.

Birge, R. R., Einterz, C. M., Knapp, H. M., & Murray, L. P. (1988) *Biophys. J. 53*, 367–385.

Boucher, F., Leblanc, R. M. (1985) *Photochem. Photobiol. 41*, 459–465.

Cooper, A. (1979) *Nature (London) 282*, 531–533.

DeGrip, W. J., Gillespie, J., Bovee-Guerts, P. H. M., & Rothschild, K. J. (1987) *Retinal Proteins*, pp 133–143, VNU Science Press, Utrecht, The Netherlands.

Derguini, F., & Nakanishi, K. (1986) *Photobiochem. Photobiophys. 13*, 259–283.

Doukas, A. G., Lu, P. Y., & Alfano, R. R. (1981) *Biophys. J. 35*, 547–550.

Doukas, A. G., Junnarkar, R. R., Alfano, R. R., Callender, R. H., & Balogh-Nair, V. (1985) *Biophys. J. 47*, 795–798.

Einterz, C. M., Lewis, J. W., & Kliger, D. S. (1987a) *Proc. Natl. Acad. Sci. U.S.A. 84*, 3699–3703.

Einterz, C. M., Lewis, J. W., & Kliger, D. S. (1987b) *Biophysical Studies of Retinal Binding Proteins* (Ebrey, T. G., Honig, B., & Frauenfelder, H., Eds.) pp 282–286, University of Illinois Press, Urbana–Champaign.

Einterz, C. M., Hug, S. J., Lewis, J. W., & Kliger, D. S. (1990) *Biochemistry* (following paper in this issue).

Eyring, G., Curry, B., Mathies, R., Fransen, R., Palings, I., & Lugtenburg, J. (1980) *Biochemistry 19*, 2410–2418.

Eyring, G., Curry, B., Broek, A., Lugtenburg, J., & Mathies, R. (1982) *Biochemistry 21*, 384–393.

Fukada, Y., Shichida, Y., Yoshizawa, T., Ito, M., Kodama, A., & Tsukida, K. (1984) *Biochemistry 23*, 5826–5832.

Golub, G. H., & Reinsch, C. (1970) *Numer. Math. 14*, 403–420.

Grellman, K. H., Livingston, R., & Pratt, D. (1962) *Nature (London) 193*, 1258–1260.

Hofrichter, J., Henry, E. R., Sommer, J. H., Deutsch, R., Ikeda-Saito, M., Yonetani, T., & Eaton, W. A. (1985) *Biochemistry 24*, 2667–2679.

Honig, B., Dinur, U., Nakanishi, K., Balogh-Nair, V., Gawinowicz, M. A., Arnaboldi, M., & Motto, M. G. (1979a) *J. Am. Chem. Soc. 101*, 7084–7086.

Honig, B., Ebrey, T., Callender, R. H., Dinur, U., & Ottolenghi, M. (1979b) *Proc. Natl. Acad. Sci. U.S.A. 76*, 2503–2507.

Hubbard, R., & Kropf, A. (1958) *Proc. Natl. Acad. Sci. U.S.A. 44*, 130–139.

Hug, S. J., Lewis, J. W., & Kliger, D. S. (1988) *J. Am. Chem. Soc. 110*, 1998–1999.

Hurley, J. B., Ebrey, T. G., Honig, B., & Ottolenghi, M. (1977) *Nature (London) 270*, 540–542.

Kliger, D. S., Horwitz, J. S., Lewis, J. W., & Einterz, C. M. (1984) *Vision Res. 24*, 1465–1470.

Lewis, J. W., Miller, J. L., Mendel-Hartvig, J., Schaechter, L. E., Kliger, D. S., & Dratz, E. A. (1984) *Proc. Natl. Acad. Sci. U.S.A. 81*, 743–747.

Lewis, J. W., Warner, J., Einterz, C. M., & Kliger, D. S. (1987) *Rev. Sci. Instrum. 58*, 945–949.

Lewis, J. W., Einterz, C. E., Hug, S. J., & Kliger, D. S. (1989) *Biophys. J. 56*, 1101–1111.

Lugtenburg, J., Muradin-Szweykowska, M., Heeremans, C., Pardoen, J. A., Harbison, G., Herzfeld, J., Griffin, R. G., Smith, S. O., & Mathies, R. A. (1986) *J. Am. Chem. Soc. 108*, 3104–3105.

Mao, B., Tsuda, M., Ebrey, T. G., Akita, H., Balogh-Nair, V., & Nakanishi, K. (1981) *Biophys. J. 35*, 543–546.

Nagle, J. F., Parodi, L. A., & Lozier, R. H. (1982) *Biophys. J. 38*, 161–174.

Ottolenghi, M., & Sheves, M. (1987) On the nature of the primary photochemical events in rhodopsin and bacteriorhodopsin, in *Primary Processes in Photobiology* (Kobayashi, T., Ed.) pp 144–153, Springer-Verlag, Berlin.

Packer, L., Ed. (1982) *Biomembranes, Part I: Visual Pigments and Purple Membranes*, Methods in Enzymology 81, Academic, New York.

Palings, I., Pardoen, J. A., van den Berg, E., Winkel, C., Lugtenburg, J., & Mathies, R. A. (1987) *Biochemistry 26*, 2544–2556.

Peters, K. S., & Leontis, N. (1982) Dynamics of the primary event in vision, *Biological Events Probed by Ultra-Fast Laser Spectroscopy* (Alfano, A. A., Ed.) pp 259–269, Academic Press, New York.

Peters, K. S., Applebury, M. L., & Rentzepis, P. M. (1977) *Proc. Natl. Acad. Sci. U.S.A. 74*, 3119–3123.

Rosenfeld, T., Honig, B., Ottolenghi, M., Hurley, J., & Ebrey, T. G. (1977) *Pure Appl. Chem. 49*, 341-351.
Rothschild, K. J., & DeGrip, W. J. (1986) *Photobiochem. Photobiophys. 13*, 245-258.
Sasaki, N., Tokunaga, F., & Yoshizawa, T. (1980) *Photochem. Photobiol. 32*, 433-441.
Schick, G. A., Cooper, T. M., Holloway, R. A., Murray, L. P., & Birge, R. R. (1987) *Biochemistry 26*, 2556-2562.
Sheves, M., Friedman, N., Albeck, A., & Ottolenghi, M. (1985) *Biochemistry 24*, 1260-1265.
Sheves, M., Albeck, A., Ottolenghi, M., Bovee-Guerts, P. H. M., DeGrip, W. J., Einterz, C. M., Lewis, J. W., Schaechter, L. E., & Kliger, D. S., (1986) *J. Am. Chem. Soc. 108*, 6440-6441.
Sheves, M., Albeck, A., Baasov, T., Friedman, N., & Ottolenghi, M. (1987) *Retinal Proteins*, pp 205-216, VNU Science Press, Utrecht, The Netherlands.
Shichida, Y. (1986) *Photobiochem. Photobiophys. 13*, 287-307.
Shichida, Y., Kropf, A., & Yoshizawa, T. (1981) *Biochemistry 20*, 1962-1968.
Shichida, Y., Matuoka, S., & Yoshizawa, T. (1984) *Photobiochem. Photobiophys. 7*, 221-228.
Spudich, J. L., McCain, D. A., Nakanishi, K., Okabe, M., Shimizu, N., Rodman, H., Honig, B., & Bogomolni, R. A. (1986) *Biophys. J. 49*, 479-483.
Suzuki, T., & Callender, R. H. (1981) *Biophys. J. 34*, 261-265.
Warshel, A., & Barboy, N. (1982) *J. Am. Chem. Soc. 104*, 1469-1476.
Yoshizawa, T., & Wald, G. (1963) *Nature 197*, 1279-1286.

Early Photolysis Intermediates of the Artificial Visual Pigment 13-Demethylrhodopsin†

Cora M. Einterz,‡ Stephan J. Hug, James W. Lewis, and David S. Kliger*
Chemistry Department, University of California, Santa Cruz, California 95064
Received June 6, 1989; Revised Manuscript Received October 3, 1989

ABSTRACT: Nanosecond time-resolved absorption measurements are reported for the room temperature photolysis of a modified rhodopsin pigment, 13-demethylrhodopsin, which contains the chromophore 13-demethylretinal. The measurements are consistent with the formation of an equilibrium between a BATHO-13-demethylrhodopsin species and a blue-shifted species (relative to the parent pigment), BSI-13-demethylrhodopsin. The results are compared to those acquired after photolysis of native bovine rhodopsin [Hug, S. J., Lewis, J. W., Einterz, C. M., Thorgeirsson, T. E., & Kliger, D. S. (1990) *Biochemistry* (preceding paper in this issue)] and to results obtained after photolysis of several modified isorhodopsin pigments in which the BSI species was first observed. It is concluded that in all of the pigments the results are consistent with the formation of an equilibrium between BATHO and BSI, which subsequently decays on a nanosecond time scale at room temperature to a lumirhodopsin intermediate.

Studies of the products created upon light absorption by rhodopsin (RHO), which consists of an 11-*cis*-retinal chromophore attached via a protonated Schiff base linkage to the protein opsin, are instrumental in elucidating the mechanism underlying the visual transduction process. At liquid nitrogen temperatures, the chromophore of RHO undergoes a photoisomerization to produce a red-shifted absorber, bathorhodopsin (BATHO). When gradually warmed in the dark, BATHO is converted successively into lumirhodopsin (LUMI), metarhodopsin I (META-I), and metarhodopsin II (META-II), and finally the retinal chromophore is released from the protein pocket. It has been shown that BATHO stores about 32 kcal/mol of the photon energy which RHO absorbs (Boucher & Leblanc, 1985; Cooper, 1979; Schick et al., 1987). At physiological temperatures it is believed that this energy is used in the propagation of conformational and structural changes which convert RHO to an activated form which triggers visual transduction.

In order to understand these transitions, many spectroscopic studies have focused on elucidating the structure of BATHO and the mechanism by which BATHO decays to the subsequent intermediates [for recent reviews, see Shichida (1986) and Ottolenghi and Sheves (1987)]. In early studies of the room temperature photolysis products of RHO, a red-shifted absorption was observed on the nanosecond time scale which was attributed to BATHO (Cone, 1972; Busch et al., 1972; Rosenfeld et al., 1972; Bensasson et al., 1975; Birge, 1981; Horwitz et al., 1983). It was believed that BATHO decayed with a lifetime on the order of 10^{-8} s to a blue-shifted intermediate, which was attributed to LUMI.

More recent time-resolved spectral studies have brought this model of a simple BATHO to LUMI transition into question (Einterz et al., 1987; Hug et al., 1988, 1990). The clear shift in the isosbestic point between absorption spectra collected from 20 to 600 ns after photolysis of RHO showed that there was more than one process occurring on the nanosecond time scale. In our original analysis of the multiexponential decay at room temperature in the nanosecond time domain, we suggested that this behavior was consistent with the parallel decay of two BATHO species to either one or two LUMI pigments (Einterz et al., 1987). This was justified in part by previous observations of two BATHO products after low-temperature photolysis of RHO by Sasaki et al. (1980a,b). However, it has recently been suggested that the time de-

† This work was supported by NIH Grant EY00983.
‡ Present address: Laboratory for Atmospheric and Space Physics, University of Colorado, Boulder, CO 80309.

0006-2960/90/0429-1485$02.50/0